PCCP

View Online
Dynamic Article Links

Cite this: DOI: 10.1039/c1cp21126a

www.rsc.org/pccp

PAPER

# SERS from two-tier sphere segment void substrates†

**Robert P. Johnson,[a] Sumeet Mahajan,[b] Mamdouh E. Abdelsalam,[a]**
**Robin M. Cole,[b] Jeremy J. Baumberg,[b] Andrea E. Russell[a] and Philip N. Bartlett*[a]**

***Received 11th April 2011, Accepted 1st August 2011***
**DOI: 10.1039/c1cp21126a**

Sphere segment void, or inverse opal, films prepared from a variety of coinage metals have shown promise as reliable and reproducible substrates for surface enhanced Raman spectroscopy (SERS). Sphere segment void substrates are prepared from colloidal templates consisting of one or more layers of polystyrene spheres. In this paper, we investigate the reflection spectra and SERS for a gold film consisting of two-tiers of spherical cavities, and show that the best SERS enhancements are obtained from substrates consisting of just a single layer of sphere segment voids.

## Introduction

Surface Enhanced Raman Spectroscopy (SERS) was first observed in 1974 for pyridine absorbed at a roughened silver electrode.[1] The observed spectra were a million fold more intense than anticipated. However, it wasn't until three years later that Van Duyne and Jeanmarie,[2] and Albrecht and Creighton[3] independently attributed this enhancement to a localized electromagnetic field at the electrode surface.

Although even today the exact mechanism by which the enhancement occurs is still subject to debate, the generally accepted theory suggests that there are two main contributory factors. Firstly, the charge transfer enhancement, which arises from the chemisorption of the adsorbate at the metal surface[4] and secondly the electromagnetic enhancement, a non-adsorbate specific enhancement arising from the focusing of the electric field *via* plasmon resonances at the metallic surface.[5] The second and larger electromagnetic enhancement relies on the presence of localised electromagnetic fields[6–9] which are strongly dependent on the morphology (structural features) of the surface at the nanoscale.[6–10]

Early substrates were often prepared by randomly roughening a metallic surface, or by using aggregated gold or silver colloid particles.[11,12] Although both these types of substrates show good enhancement they are plagued with poor reproducibility as only certain positions, known as nanoscale 'hot spots', have the correct localised electromagnetic fields to give a significant enhancement.

Recent advances in nanoscale lithography have led to a wide variety of 'rationally designed' SERS substrates prepared by structuring of coinage metals on the nano-scale. These types of substrate provide much better reproducibility than randomly roughened surfaces or colloids. A plethora of examples exist in the literature, including nanorings,[13] nanotriangles,[14] spherical nanoshells,[15,16] nanopits[17] and nanotip arrays.[18]

Research in our group has led to the development of the sphere segment void (SSV) substrate; a thin layer metallic film with a regular array of spherical cavities.[6,9,10,19–21] The substrate is prepared *via* electro-deposition of a coinage metal, commonly gold, through a monolayer of hexagonally close packed polystyrene spheres of a chosen size, and followed by dissolution of the polystyrene to leave an all metal inverse sphere structure. As shown in our earlier work, by correctly choosing both the sphere size and the deposition height through the template[9,21,22] it is possible to obtain a tuneable electromagnetic enhancement with ~10% standard deviation in enhancement[10,23] across the surface.

A number of groups have shown that SERS can be obtained from inverse opal structures prepared from multiple layers of close packed spheres.[24–26] However, in these reports the precise number of layers is often left uncontrolled, the internal surfaces were rough, and the geometry of the top surface was not systematically controlled. The effect of the number of spherical voids layers on the properties of the final substrate has not been studied. In this paper a sphere segment void (SSV) substrate is prepared using a colloidal template consisting of just two layers of close packed 600 nm polystyrene spheres using electrodeposition to produce a structure with smooth walls. The thickness of the substrate was systematically varied so that multiple deposition thicknesses were present on the same substrate, allowing the optical and SERS properties to be easily compared for a variety of controlled thicknesses and surface morphologies.

We show that the optimal SERS enhancement for a two-tier cavity substrate occurs when the structural morphology of the top layer is similar to that which provides the best enhancement for a single tier cavity substrate. However, despite the fact that

---

[a] *School of Chemistry, University of Southampton, Highfield, Southampton SO17 1BJ, UK. E-mail: pnb@soton.ac.uk; Fax: + 44-23-8059-3781; Tel: + 44-23-8059-2373*
[b] *Nanophotonics Centre, Cavendish Laboratory, University of Cambridge, Cambridge CB3 0HE, UK*

† Electronic supplementary information (ESI) available: Angle-resolved reflectance maps. See DOI: 10.1039/c1cp21126a

the number of molecules in the laser spot is 2 to 3 times greater we find that the maximum enhancement obtained for the two-tier substrate is only about half that which can be achieved with a single tier substrate. We suggest, based on the strong similarities in the reflection spectra, that this is because the electromagnetic fields that give rise to the SERS enhancement are generated only by structural features on the upper most layer of the two-tier sphere segment void substrate. The approximately 50% decrease in the maximum SERS intensity on the two-tier substrate is then interpreted in terms of the extra holes that are present in the second layer of cavities through contact with the underlying layer and the increased number of template packing defects in the second layer leading to greater disorder in the structure. The best SERS enhancements are thus achieved using substrates prepared from a just a single layer of polystyrene spheres.

## Experimental

All reagents used were analytical grade and obtained from Sigma-Aldrich unless stated otherwise.

### Fabrication of opal templates

Two-tier SSV substrates were prepared in a two step process. Firstly, a monolayer of polystyrene spheres is prepared on a gold surface, as described by our group previously, then a second layer of polystyrene spheres is deposited to form a bi-layer template.

For a typical fabrication procedure, glass microscope slides were coated with a 10 nm chromium adhesion layer followed by 200 nm of gold using standard thermal evaporation. 2 cm × 1.5 cm pieces were cut from the gold-coated slide and cleaned by sonication in isopropanol for 90 min. Subsequently, these treated surfaces are washed with water. The gold surface is used to construct a thin fluid cell consisting of the gold surface itself, a glass cover slip and sidewall made from a thin 300 μm spacer layer of Parafilm® (Pechiney-Plastic). The thin fluid cell is filled with 600 nm polystyrene spheres (obtained as 1% wt. solution from Duke Scientific). Slow evaporation of the solution from the cell results in assembly of a monolayer of hexagonally close packed polystyrene spheres.

The monolayer template was rinsed with deionised water to remove any surfactants left behind during template formation and the thin fluid cell reconstructed utilising the monolayer template on gold, a glass cover slip and sidewall made from a thin 300 μm spacer layer of Parafilm®. Next, the thin fluid cell was refilled with polystyrene sphere solution and the slow evaporation procedure repeated to form a second layer of spheres on top of the first.

### Preparation of spherical cavity gold films

Spherical cavity films were prepared by electrodeposition through the two-tier template. Electrodeposition was carried out using a sulfite-based commercial gold electroplating bath (ECF 60, Metalor) to which an additive (Brightener E3, Metalor) was added for a bright and smooth finish. During electrodeposition the brightener acts as a catalyst,[27] enhancing the nucleation of gold, preventing an uneven deposit and ensuring that the deposited metal is a true cast of the polystyrene template. Electrodeposition was performed using a conventional three electrode system at a constant potential of −0.72 *vs.* SCE. The thickness of the metal deposited was controlled by monitoring the charge passed during the electrodeposition. Samples were prepared with steps in thickness along the length of the template by incrementally removing the glass slide from the plating bath in steps of 500 μm.

The structure and quality of the sculpted gold films were confirmed using two environmental scanning electron microscopes; a Philips XL30 and a Phillips JSM 6500.

### Reflectance measurements

Reflectance spectra at normal incidence were recorded using a BX51 TRF Olympus optical microscope. The samples were illuminated by an incoherent white light source and the images were recorded using a CCD camera (DP2 Olympus). A fibre-coupled spectrometer (Ocean Optics, spectral range 300–1000 nm, 40x magnification) placed in a focal plane of the image was used to record the spectral response from the selected area with a spot size of 50 μm. Spectra were normalised relative to flat gold.

The dispersion of the plasmons on the substrate was investigated by recording the reflectivity spectra at an incident angle range of 0–60° (varying the momentum of the incident photons). The sample was mounted on a custom-built goniometer and spectra were recorded from a 50 μm spot with both infrared and visible spectrometers (Ocean Optics, USB2000 and NIR512). Custom-built software was used to control both the goniometer and the spectrometers. Spectra were normalised relative to flat gold. Data was collected for both TE polarised (transverse electric) and TM polarised (transverse magnetic) light. A polariser was used to control whether TM or TE light was incident on the sample for a given measurement.

### Raman measurements

Raman spectra were collected using a Renishaw Raman 2000 system with a 633 nm HeNe laser. Spectra were collected using the extended scanning mode from 400 to 3200 $\mathrm{cm^{-1}}$ and a 10 s accumulation time. A × 50 objective was used (numerical aperture 0.75), providing a 5 μm spot at the sample. A laser power of 1.5 mW was measured at the sample.

The gold structures were coated with a monolayer of benzene thiol by soaking in a 10 mM solution in ethanol for 1 h. The substrates were then rinsed with ethanol and water, and dried under a stream of argon. Previous work on the modification of the surfaces of inverse opal gold films of the type described here has show that solution modification of the surface uniformly coats the entire surface of the structure (both outer and inner cavities) with a monolayer of adsorbed species.[28–31]

## Results and discussion

### Structural morphology of the two-tier film

A two-tier inverse opal film, graded in 500 μm steps of incremental height 0.1d (60 nm) along its length was prepared as described in the Experimental Section. The structural morphology of the two-tier film was characterised in detail with scanning electron microscopy (SEM).

At low deposition thicknesses, *i.e.* less than 0.7d (420 nm), the observed surface morphology is identical to that seen for single layer inverse opal structures.[6] Each window connects the void to its six neighbours in the plane about the point at which the spheres in the template came into contact. From previous work using a double templating technique[32] we find that these interconnections are a result of the inability of electrodeposition to fill the narrow regions around the contact points between the separate spheres in the template.

For deposition thicknesses between $\sim$0.8d and $\sim$1.1d (shaded in Fig. 2) the structural morphology of the film changes dramatically. This is the 'cross-over' region, *i.e.* the range in thicknesses in which there is an obvious effect from the presence of the second layer of template spheres, but where the first layer of spheres is not completely encapsulated. Between approximately 0.8d and 0.9d, the spherical voids from the first layer become elongated at three points, which correspond to the three points at which the template sphere in the first layer touches the three template spheres in the second layer in the hexagonal close packed arrangement. In Fig. 1b it is possible to see the indents in the gold surface left by the second layer of spheres. Between approximately 1.1d and 1.6d, the structure of the film consists of an upper layer of sphere segment voids, each one connected in three places to spherical voids in the lower layer (Fig. 1c).

The morphology of the upper layer of the voids for the thickness range 1.2d–1.6d varies in the same way as for the lower layer of voids for the thickness range 0.3–0.7d (Fig. 2). In this range, the morphology at a given thickness in the upper layer has a corresponding morphology at a given thickness in the lower layer (at its thickness minus 0.87d).

Fig. 1d also highlights the presence of a defect unique to films constructed from templates with two or more layers of spheres, the Shockley partial,[33] highlighted by arrow B. This frequently occurring defect in close packed arrays is caused when there is a packing error in the lower layer, but which is not carried over into the second layer. The consequence of this is that the spherical voids in the second layer only connect to two voids in the second layer, instead of the usual three.

The SEM images in Fig. 1 highlight the clear difficulty in producing high quality, and defect free, nanostructures from multiple layers of polystyrene spheres by sequential template deposition. As additional layers of spheres are added, the presence of defects increases and thus the morphology becomes less regular with each additional layer.

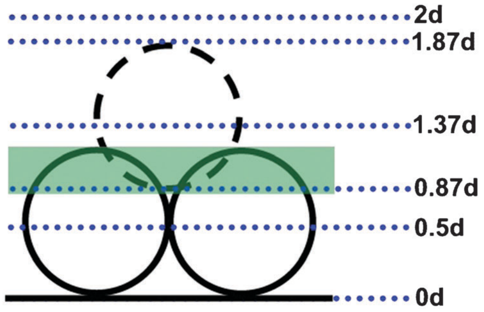

**Fig. 2** Schematic highlighting the hexagonal close packing arrangement of 600 nm colloidal particles.

## SERS and optical properties of two-tier films

As reported previously,[9] monolayer inverse opal films are highly tunable, and by correctly choosing both the sphere size and the deposition height through the template, it is possible to obtain both significant and reproducible electromagnetic enhancements for a chosen excitation wavelength. Typically, average enhancements of $10^6$ can be achieved for a 633 nm excitation source when the film is prepared at a thickness of 0.75d and a sphere diameter of 600 nm is used.[10] To determine what affect adding a second tier to the inverse opal film would have on the SERS enhancement, a monolayer of benzene thiol was adsorbed onto the surface and a number of spectra were acquired as a function of film height. The intensity of the $C{=}C$ aromatic ring stretch[34] at 1075 $cm^{-1}$, corrected for the background, is plotted as a function of film height in Fig. 3. As we can see from the spectra in Fig. 3A the background intensity follows that of the SERS bands. This is in agreement with our previous work and arises because of the common plasmonic origin of the SERS signal and background.[35,36]

The optimal film height for SERS enhancement from the two-tier film is approximately 0.7d. This is nearly identical to that observed for monolayer inverse opal films previously. At this film thickness the structural morphology and regularity is determined purely from the lower layer of colloidal particles that form the template. The next optimal film height for SERS enhancement is approximately 1.4d. At this thickness the surface morphology of the outer cavities is close to that of the cavities in the 0.7d structure, but with extra windows through to the lower spherical voids puncturing the upper sphere segment voids as seen in Fig. 1c.

Despite the fact that there are 2 to 3 times as many benzene thiol molecules in the illuminated region for the 1.4d structure as compared to the 0.7d structure due to the molecules

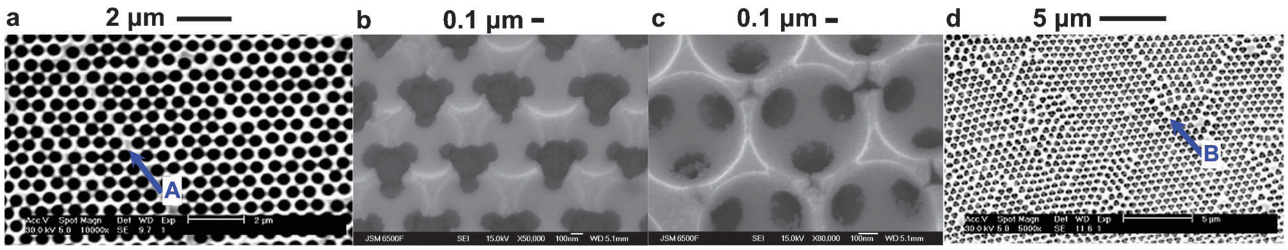

**Fig. 1** SEM images of the two-tier spherical cavity film at thicknesses (a) 0.5d (b) 1.0d (c) 1.3d and (d) 1.5d (d = 600 nm). Commonly occurring defects are highlighted by arrows (A) shrinkage and (B) Shockley partial.

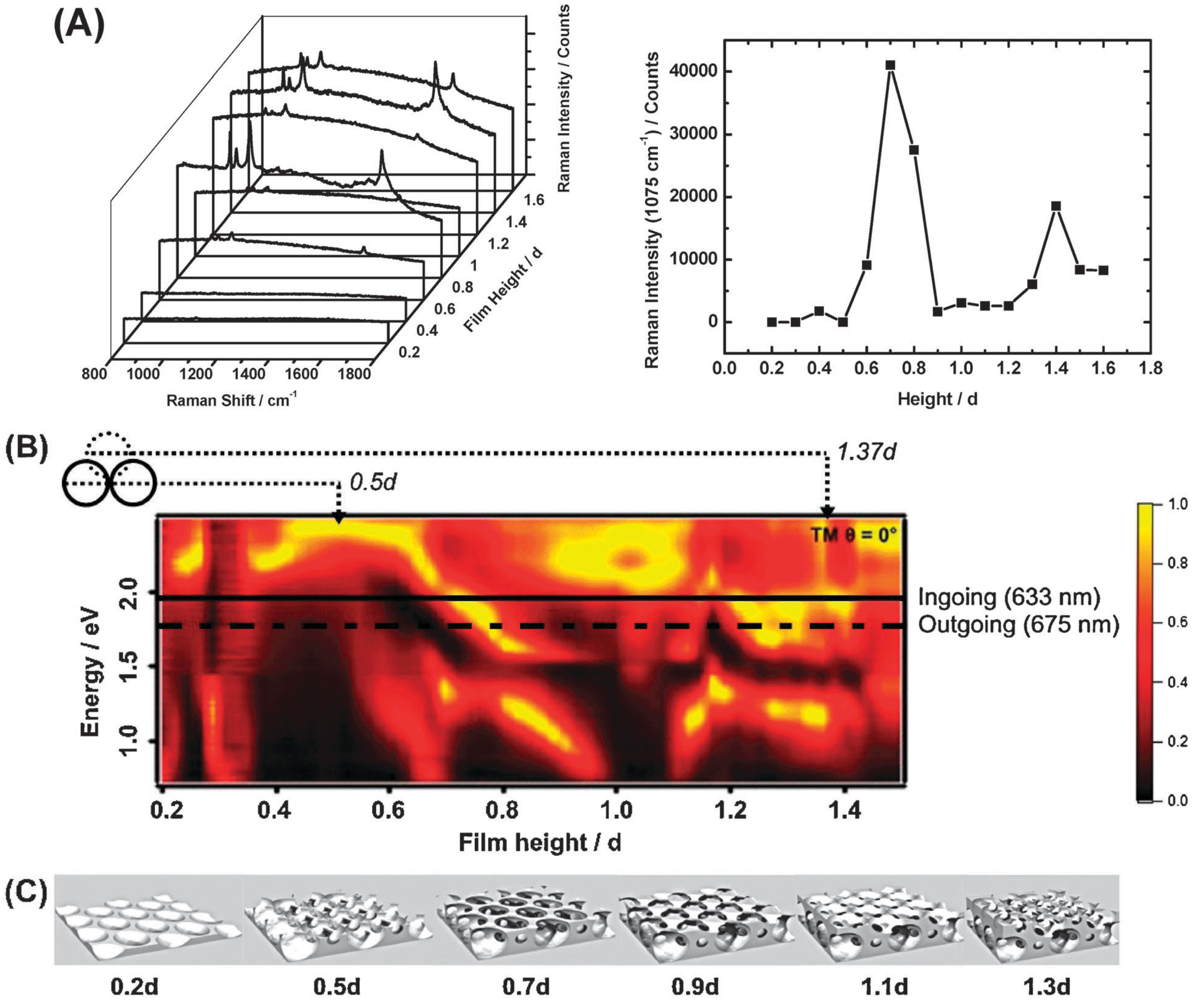

**Fig. 3** (A) Raman data illustrating the change in SERS intensity of an adsorbed benzene thiol layer with film height. The plot on the right shows the background corrected SERS intensity for the 1075 cm$^{-1}$ benzene thiol band as a function of the gold film thickness. (B) Optical reflectance data at normal incidence, showing plasmon absorption energies as a function of film thickness, normalised to flat gold. Yellow is strongest absorption, black is weakest absorption. Angle resolved optical data is available in the Supporting Information). (C) Structure of the double layer template at varying film heights.

adsorbed on the surface of the inner layer of cavities the SERS intensity for the 1.4d structure is only half that for the 0.7d structure indicating that only the top layer of voids contributes to the enhancement. The lower SERS intensity for the 1.4d structure can be explained in large part by the fact that the sphere segment voids in the top tier have a lower surface area because of the three windows connecting them to the voids in the bottom layer. The calculated surface area for each cavity in the 0.7d structure is 0.56 μm$^2$. The calculated surface area for each outer cavity in the 1.4d structure, assuming that the windows that connect the upper sphere segment cavity to the three spherical cavities in the inner layer have a radius of 100 nm (based on the SEM images), is 0.34 μm$^2$, 40% less that for the 0.7d structure.

This decrease in the surface area for the outer sphere segment cavities, and thus in the number of benzene thiol molecules exposed in the outer cavities in the laser spot, accounts for most of the decrease in SERS intensity seen in Fig. 3A. The additional slight decrease in SERS intensity for the 1.4d structure can be accounted for by the increase in the number of packing defects in the template, which leads to defects on the 10 s to 100 s on nanometre scale in the packing in the void structure as seen in the SEM (Fig. 1).

The Raman data acquired was augmented by optical reflectivity measurements obtained as a function of film height. Measurements at normal incidence are shown in Fig. 3B. Angle resolved reflectance maps and the reflectance spectra at normal incidence are given in the Supplementary Information.† The data clearly show the movement of the absorption maxima (indicated by yellow) as a function of film height. At 0.7d and at 1.4d, the absorption maxima are centred around 633 nm, which corresponds to the ingoing (pump) wavelength for the Raman. However, to maximise SERS enhancement absorption must also be strong at the outgoing wavelength.

In the case of the benzene thiol peak at 1075 cm$^{-1}$ this corresponds to a wavelength of 675 nm, and this also occurs when the film height is around 0.7d and 1.4d due to the plasmon mode dispersion.

From the reflectance map it is also evident that the plasmon modes are not so well defined when the film thickness reaches the second layer of inverse opals, *i.e.* $>0.8$d. This can be attributed to the increasing number of packing defects in the film morphology, and more importantly due to the effect of void punctures. The images in Fig. 3C show representations of films of different thickness showing the effect on the void structure and top surface as thickness increase through the two layer template.

## Conclusions

For two-tier sphere segment void substrates the maximum SERS enhancement occurs when the morphology of the outer layer of cavities closely matches that of the optimum structure for SERS enhancement for the single layer. In this case the reflectance spectra for the two, the optimum two-tier and the single layer structures, are closely similar indicating similar plasmonics. However, the SERS intensity observed for the optimum two-tier structure is only about one half that on the optimum single layer structure despite the fact that there are 2 to 3 times as many molecules in the laser illuminated region when adsorption on the walls of the inner and outer cavities is taken into account. These results indicate that the electromagnetic enhancement is restricted to the outer layer of the structure and that there is no benefit for SERS in increasing the thickness of the structure beyond a single layer.

The reduction in SERS intensity for the optimum two-tier structure by about half is accounted for mainly by the reduction in surface area of the outer cavities, relative to the corresponding single layer structure, as a result of the three windows which connect each outer cavity to the three inner cavities below and, to a lesser extent, by the increase in disorder in the packing of the cavities.

## Notes and references

1 M. Fleischmann, P. J. Hendra and A. J. McQuillan, *Chem. Phys. Lett.*, 1974, **26**, 163–166.
2 D. L. Jeanmaire and R. P. Van Duyne, *J. Electroanal. Chem.*, 1977, **84**, 1–20.
3 M. G. Albrecht and J. A. Creighton, *J. Am. Chem. Soc.*, 1977, **99**, 5215–5217.
4 A. Campion, J. E. Ivanecky, C. M. Child and M. Foster, *J. Am. Chem. Soc.*, 1995, **117**, 11807–11808.
5 F. W. King, R. P. Van Duyne and G. C. Schatz, *J. Chem. Phys.*, 1978, **69**, 4472–4481.
6 P. N. Bartlett, J. J. Baumberg, S. Coyle and M. E. Abdelsalam, *Faraday Discuss.*, 2004, **125**, 117–132.
7 T. A. Kelf, Y. Sugawara, R. M. Cole, J. J. Baumberg, M. E. Abdelsalam, S. Cintra, S. Mahajan, A. E. Russell and P. N. Bartlett, *Phys. Rev. B: Condens. Matter Mater. Phys.*, 2006, **74**, 245415.
8 R. M. Cole, J. J. Baumberg, F. J. Garcia de Abajo, S. Mahajan, M. Abdelsalam and P. N. Bartlett, *Nano Lett.*, 2007, **7**, 2094–2100.
9 S. Mahajan, R. M. Cole, B. F. Soares, S. H. Pelfrey, A. E. Russell, J. J. Baumberg and P. N. Bartlett, *J. Phys. Chem. C*, 2009, **113**, 9284–9289.
10 S. Cintra, M. E. Abdelsalam, P. N. Bartlett, J. J. Baumberg, T. A. Kelf, Y. Sugawara and A. E. Russell, *Faraday Discuss.*, 2006, **132**, 191–199.
11 P. C. Lee and D. Meisel, *J. Phys. Chem.*, 1982, **86**, 3391–3395.
12 K. C. Grabar, R. G. Freeman, M. B. Hommer and M. J. Natan, *Anal. Chem.*, 1995, **67**, 735–743.
13 J. Aizpurua, P. Hanarp, D. S. Sutherland, M. Kall, G. W. Bryant and F. J. Garcia de Abajo, *Phys. Rev. Lett.*, 2003, **90**, 057401.
14 C. L. Haynes and R. P. Van Duyne, *J. Phys. Chem. B*, 2003, **107**, 7426–7433.
15 S. J. Oldenburg, R. D. Averitt, S. L. Westcott and N. J. Halas, *Chem. Phys. Lett.*, 1998, **288**, 243–247.
16 J. B. Jackson and N. J. Halas, *Proc. Natl. Acad. Sci. U. S. A.*, 2004, **101**, 17930–17935.
17 N. M. B. Perney, J. J. Baumberg, M. E. Zoorob, M. D. B. Charlton, S. Mahnkopf and C. M. Netti, *Opt. Express*, 2006, **14**, 847–857.
18 N. C. Linn, C. H. Sun, A. Arya, P. Jiang and B. Kiang, *Nanotechnology*, 2009, **20**, 225303.
19 M. E. Abdelsalam, S. Mahajan, P. N. Bartlett, J. J. Baumberg and A. E. Russell, *J. Am. Chem. Soc.*, 2007, **129**, 7399–7406.
20 L. Cui, S. Mahajan, R. M. Cole, B. Soares, P. N. Bartlett, J. J. Baumberg, I. P. Hayward, B. Ren, A. E. Russell and Z. Q. Tian, *Phys. Chem. Chem. Phys.*, 2009, **11**, 1023–1026.
21 S. Mahajan, M. Abdelsalam, Y. Suguwara, S. Cintra, A. Russell, J. Baumberg and P. Bartlett, *Phys. Chem. Chem. Phys.*, 2007, **9**, 104–109.
22 S. Mahajan, J. Richardson, N. B. Gaied, Z. Zhao, T. Brown and P. N. Bartlett, *Electroanalysis*, 2009, **21**, 2190–2197.
23 M. E. Abdelsalam, P. N. Bartlett, J. Baumberg, S. Cintra, T. Kelf and A. E. Russell, *Electrochem. Commun.*, 2005, **7**, 740–744.
24 D. M. Kuncicky, B. G. Prevo and O. D. Velev, *J. Mater. Chem.*, 2006, **16**, 1207–1211.
25 L. Lu and A. Eychmüller, *Acc. Chem. Res.*, 2008, **41**, 244–253.
26 P. M. Tessier, O. D. Velev, A. T. Kalambur, J. F. Rabolt, A. M. Lenhoff and E. W. Kaler, *J. Am. Chem. Soc.*, 2000, **122**, 9554–9555.
27 P. Wilkinson, *Gold Bull.*, 1986, **19**, 75–81.
28 S. Ben-Ali, D. A. Cook, P. N. Bartlett and A. K, *J. Electroanal. Chem.*, 2005, **579**, 181–187.
29 S. Ben-Ali, D. A. Cook, S. A. G. Evans, P. N. Bartlett and A. Kuhn, *Electrochem. Commun.*, 2003, **5**, 747–751.
30 R. Szamocki, S. Reculusa, S. Ravaine, P. N. Bartlett, A. Kuhn and R. Hempelmann, *Angew. Chem., Int. Ed.*, 2006, **45**, 1317–1321.
31 R. Szamocki, A. Velichko, F. Mücklich, S. Reculusa, S. Ravaine, S. Neugebauer, W. Schuhmann, R. Hempelmann and A. Kuhn, *Electrochem. Commun.*, 2007, **9**, 2121–2127.
32 M. A. Ghanem, P. N. Bartlett, P. de Groot and A. Zhukov, *Electrochem. Commun.*, 2004, **6**, 447–453.
33 A. Kelly and G. W. Groves, *Crystalography and Crystal Defects*, Longmann, Bristol, 1970.
34 S. W. Han, S. J. Lee and K. Kim, *Langmuir*, 2001, **17**, 6981–6987.
35 C. Farcau and S. Astilean, *Chem. Commun.*, 2011, **47**, 3861–3863.
36 S. Mahajan, R. M. Cole, J. D. Speed, S. H. Pelfrey, A. E. Russell, P. N. Bartlett, S. M. Barnett and J. J. Baumberg, *J. Phys. Chem. C*, 2010, **114**, 7242–7250.